Materials Today Bio 15 (2022) 100281

Contents lists available at ScienceDirect

Materials Today Bio

journal homepage: www.journals.elsevier.com/materials-today-bio

Label-free electrical monitoring of nucleic acid amplification with integrated hydrogel ionic diodes

Chenwei Xiong [a], Jie Li [a], Luyao Li [a], Long Chen [a,b,c], Rong Zhang [a], Xianqiang Mi [b,c,d,e,f,**], Yifan Liu [a,*]

[a] Division of Chemistry and Physical Biology, School of Physical Science and Technology, ShanghaiTech University, Shanghai, 201210, China
[b] Shanghai Advanced Research Institute, Chinese Academy of Sciences, Shanghai, 201210, China
[c] University of Chinese Academy of Sciences, Beijing, 100049, China
[d] Key Laboratory of Functional Materials for Informatics, Shanghai Institute of Microsystem and Information Technology, Chinese Academy of Sciences, Shanghai, 200050, China
[e] Key Laboratory of Systems Biology, Hangzhou Institute for Advanced Study, University of Chinese Academy of Sciences, Chinese Academy of Sciences, Hangzhou, 310024, China
[f] Key Laboratory of Systems Health Science of Zhejiang Province, Hangzhou Institute for Advanced Study, University of Chinese Academy of Sciences, Hangzhou, 310024, China

ARTICLE INFO

Keywords:
Hydrogel
Ionic diode
Electrical biosensor
Nucleic acid
Point-of-care

ABSTRACT

We demonstrate here for the first time the utility of a monolithically integrated hydrogel ionic diode for label-free quantitative DNA detection and real-time monitoring of nucleic acid amplification. The hydrogel ionic diode presented herein, unlike nanomaterial-based field-effect biosensors, features high cost-effectiveness and convenient fabrication. This is realized by patterning a micrometer-sized heterojunction consisting of adjacent segments of polycationic and polyanionic hydrogels on a microfluidic chip through simple photocuring steps. The integrated diode rectifies ionic currents being sensitive to the charge of DNA adsorbed onto the polycationic chains through electrostatic associations. Based on the mechanism, we show that the ionic biosensor can electrically quantify DNA in a dynamic range relevant to typical nucleic acid amplification assays. Utilizing the device, we demonstrate the evaluation of a PCR assay amplifying a 500-bp DNA fragment of *E. coli*, an infection-causing pathogen, and real-time *in situ* monitoring of an isothermal assay amplifying *E. coli* whole genome. We anticipate that the device could potentially pave the way for miniaturized optics-free platforms for quantifying nucleic acid amplification at point-of-care.

1. Introduction

Point-of-care diagnosis of infectious disease is essential to global healthcare, particularly in the current era of Coronavirus Disease 2019 (COVID-19) [1–3]. The identification of such infections largely relies on specific and sensitive detection of nucleic acids of their causing pathogens (e.g., bacteria and viruses), which necessitates pre-amplification of target sequences for both well-established clinical testing [4] and cutting-edge biomedical research [5]. To date, a wealth of nucleic acid amplification techniques have been broadly applied, such as polymerase chain reaction (PCR) [6], recombinase polymerase amplification (RPA) [7], and multiple displacement amplification (MDA) [8]. Monitoring the progress of such assays is critical to determining the existence and levels of target nucleic acids, which typically incorporates fluorescent reporter probes and optical quantification means [9,10]. However, the fluorescent reagents may pose inhibitory effects to the reactions [11]. Further, it is daunting to integrate the sophisticated and expensive optical readout instrumentation into a miniaturized device for point-of-care diagnosis. Such concerns have elicited an urgent need to monitor nucleic acid amplification through non-optical means.

Electrical detection of nucleic acids based on their intrinsic charge has drawn growing attention due to the label-free nature and ease in electrical readout measurement. A straightforward way to sense the charge of biomolecules is by utilizing electrostatic field-effect interactions between

* Corresponding author.
** Corresponding author. Key Laboratory of Functional Materials for Informatics, Shanghai Institute of Microsystem and Information Technology, Chinese Academy of Sciences, Shanghai, 200050, China.
E-mail addresses: mixq@mail.sim.ac.cn (X. Mi), liuyf6@shanghaitech.edu.cn (Y. Liu).

https://doi.org/10.1016/j.mtbio.2022.100281
Received 29 March 2022; Received in revised form 4 May 2022; Accepted 5 May 2022
Available online 11 May 2022

the molecules and the sensing surfaces [12]. Toward this goal, an assortment of electrical biosensors has been developed, such as field-effect transistors [13–15] and ionic diodes [16]. A field-effect transistor detects the charge of nucleic acids by monitoring the gated transport characteristics induced by the field effect of the molecules immobilized on the channel surfaces through hybridization or electrostatic adsorption [12]. To achieve desired detection limit, such devices are typically built on nanometer-sized structures such as nanowires [17], nanosheets [18], and fluidic nanochannels [16,19]. Notably, Ganguli et al. reported a crumpled graphene transistor for DNA amplification detection through an induced Dirac voltage shift [20]. We previously developed an integrated ionic field-effect transistor based on cylindrical nanocapillaries and demonstrated field-effect modulation of the DNA translocation [21]. Ionic diodes refer to biological or artificial ion channels that exhibit ionic current rectification, and the adsorption of charged biomolecules can be recognized by modulated surface charge density that reflects on a tuned rectification [22]. Wu et al. reported the modulation of ionic current rectification in polymer-based conical nanochannels by immobilized DNA architectures [23]. Although these field-effect devices exhibit intriguing potential in the electrical detection of nucleic acids, specific issues must be addressed before they can be practically applied, especially problems in robustness, manufacturability, and cost-effectiveness. For instance, while such devices are susceptible to the target analyte, they suffer from severe non-specific signals and environmental interferences [24]. Besides, the fabrication of these nanostructured devices may leverage low-throughput and expensive high-resolution techniques such as e-beam lithography [25]. A simple, robust, and cost-effective strategy for electrical quantification of nucleic acid amplification is to be explored.

Recently, hydrogels and relevant ionic devices have emerged as versatile building blocks of ionic circuits for diverse bioinspired applications [26]. A representative hydrogel-based ionic device is a polyelectrolyte ionic diode featuring a heterojunction comprising two oppositely charged polyelectrolyte hydrogels (polycationic and polyanionic). Han et al. reported the first demonstration of integrated polyelectrolyte diode and prototypes of logic gate circuits in 2009 [27]. More recently, Lee et al. proposed a stretchable ionic diode with mechanically modified polyelectrolyte hydrogels, which exhibited rectifying behaviors under uniaxial stretching and sustained their performance at repetitive deformations [28]. Lim et al. developed an open-junction hydrogel-based ionic diode to perform an ion-to-ion amplification [29]. The ionic current rectification in such hydrogel-based ionic diodes arises from the asymmetric electrostatic impact of the charged hydrogel backbone on the electrolyte solution, thus being extremely sensitive to the charge density of the hydrogel surface – an essential requirement of charge-based biosensors. Moreover, such devices are highly cost-effective and manufacturable as polyelectrolyte hydrogels are inexpensive and can be conveniently shaped with a standard UV (365 nm) lithography [28]. Considering these features, hydrogel-based ionic diodes are desired platforms for electrical biosensing. Nevertheless, charged-based detection of biomolecules, particularly nucleic acids, has not yet been demonstrated using these ionic devices. This study presents a quantitative and straightforward approach to monitoring nucleic acid amplification using polyelectrolyte hydrogel ionic diodes. The ionic diode used herein is a monolithically integrated microchip accommodating a heterogeneous junction composed of two adjacent segments of polycationic and polyanionic hydrogels. The biosensing concept is briefly described in Fig. 1. Due to the positively charged chains, anions predominantly fill the polycationic hydrogel to neutralize the intrinsic charge [16,30]. By contrast, cations are accumulated in the polyanionic gel. Analogous to semiconductor electronics, we abbreviate polycationic and polyanionic hydrogels as *N*-type and *P*-type, respectively. The asymmetric ion distribution within the hydrogel junction leads to a reasonable level of ionic current rectification. Once the negatively charged DNA molecules are introduced to the *N*-type gel, they are adsorbed onto the polycationic chains due to electrostatic interactions. The electrostatic adsorption decreases the net charge of the hydrogel backbones and affects the ion distribution within the *N*-type gel, which leads to weakened ionic current rectification. As a result, the ionic diode will instantly display a modulated current-voltage (*I–V*) characteristic. We determine that the change in rectification occurs at a rate commensurate with DNA mass concentration. Therefore, by constantly monitoring the overall rectification level, the ionic diode can monitor the existence and concentration of nucleic acids in real-time. Notably, the obtained dynamic range aligns with the DNA levels in common amplification reactions. Upon DNA detection, ionic rectification of the device can be readily refreshed to its original state by simply exposing it to positively charged poly-L-lysine (pLL). We apply the approach to PCR amplification of a 500-bp segment of the *E. coli* genome and achieve simple electrical monitoring of the progress of the amplification. Further, we integrate the ionic diode with a 2-μL microreactor and demonstrate *in situ* monitoring of an isothermal assay amplifying the *E. coli* whole genome.

2. Materials and methods

2.1. Device fabrication

The process of fabricating the integrated hydrogel ionic diode device is detailed in Fig. S1. Overall, the process includes fabricating the microfluidic chip and patterning the hydrogel heterojunction. The device layout was first designed with AutoCAD and printed as a plastic film mask. To fabricate the chip, a 50-μm layer of photoresist (SU8-3025, Microchem) was spin-coated onto a 3-inch silicon wafer. After a prebaking step (95 °C for 20 min), photolithography was performed under a UV light (Thorlabs COP1-A, 200 s at the highest intensity). The wafer was then post-baked at 95 °C for 8 min and developed to obtain the patterned structure. The fabricated silicon mold was stored in a petri dish. Polydimethylsiloxane (PDMS, Dow Corning SYLGARD 184) mixture was prepared by stir-mixing its precursor with a curing agent at 10:1 (w:w). The prepared PDMS mixture was poured over the mold and cured at 60 °C overnight. PDMS was peeled off from the mold and cut into individual slabs. Inlet and outlet ports were created using a custom-made hole puncher. At last, the slabs were bonded to glass slides (100-μm thick) with the assistance of oxygen plasma treatment.

Polyelectrolyte hydrogel junctions were formed on as-fabricated microfluidic chips through a two-step photocuring process. First, the microchannels were treated with a solution of 3-(trimethoxysilyl)propyl methacrylate, methanol, and acetic acid (mixed at 1:8.5:0.5 by weight) for 5 min and then washed with methanol. Next, the channels were filled with a *P*-type gel pre-solution and subjected to a photocuring process (a duration of 10 s) under a spot-lamp (Dymax 38,465). The chip was covered with a chromium glass dark mask with a 100-μm wide bright-line aligned right at the channel junction during the curing process. After thorough washing with 10 mM KCl solution, the photocuring process was repeated with an *N*-type gel pre-solution. The hydrogel pre-solutions consist of 20 wt% monomer (3-sulfopropyl acrylate potassium salt for *P*-type gel and diallyl-dimethylammonium chloride for *N*-type gel), 1 wt% crosslinker (N,N′-methylenebisacryl-amide), and 0.2 wt % photo-initiator (lithium phenyl-2,4,6-trimethyl-benzoyl phosphinate) in water. The fabricated devices were filled with a homebrew PCR buffer before further testing.

2.2. PCR and MDA assays

All PCR experiments were conducted using a real-time PCR system (BioRad CFX96). To obtain DNA fragments of various lengths, three primer pairs were designed to target 200, 500, and 800 bp segments on the *E. coli* genome, respectively. The primer sequence information follows forward primers: GCCTGAGCGAGACGAAATAC for 200 bp, GAATACCCCGATTGGTGATG for 500 bp, TCCCGCGAAATTAATACGAC for 800 bp; reverse primers: TTATGCCTCTTCCGACCATC for 200 bp, ATTCTCACCGGATTCAGTCG for 500 bp, CTTTCGGGCTTTGTTAGCAG

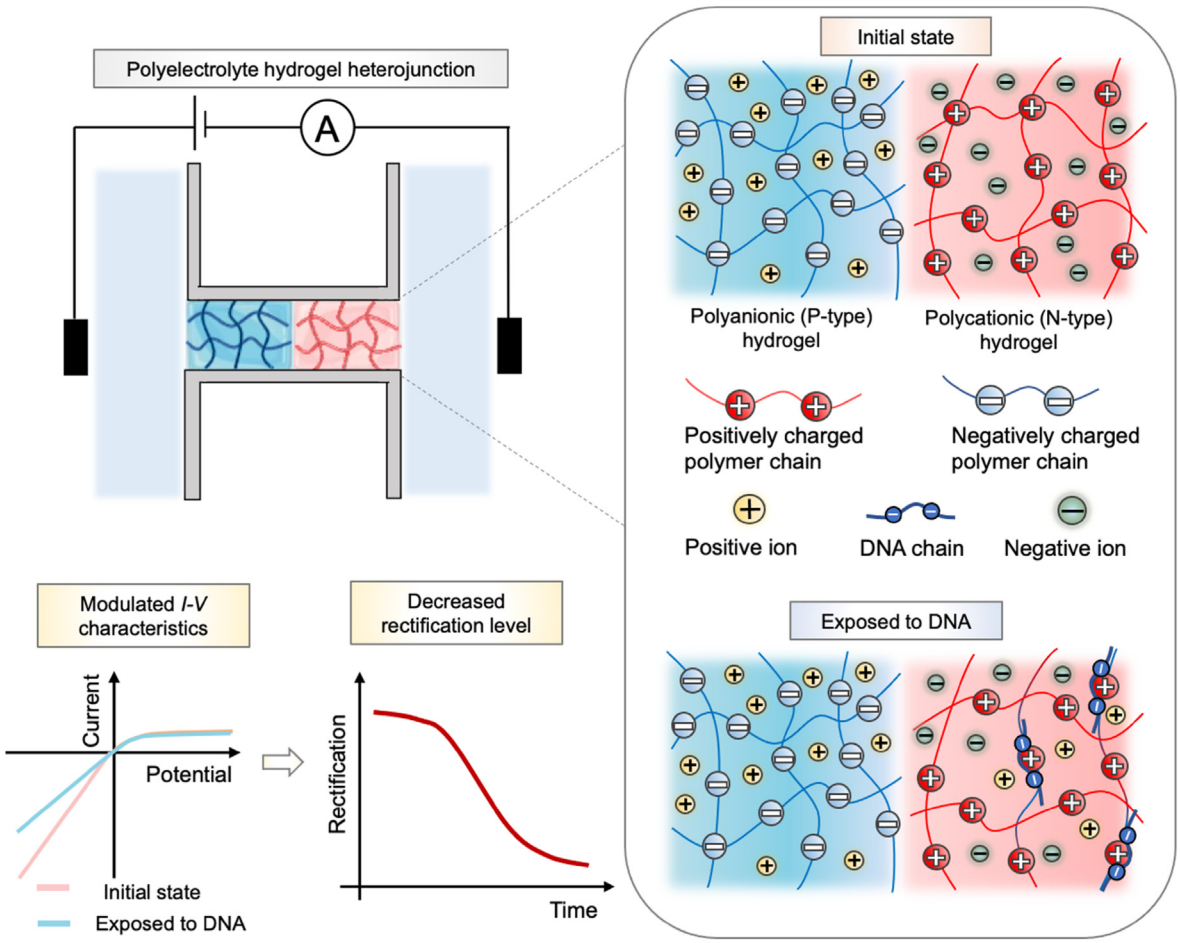

Fig. 1. Schematic overview of the hydrogel ionic diode biosensor principle. Electrical detection of DNA based on its intrinsic negative charge is realized through monitoring the modulated ionic rectification behavior induced by electrostatic adsorption of DNA molecules to oppositely charged polycationic hydrogel of the ionic diode.

for 800 bp. For all PCRs in this study, the thermal cycling condition is 95 °C for 30 s, 30 cycles of 95 °C for 15 s, 56 °C for 15 s, and 72 °C for 3 min, followed by a final extension at 72 °C for 5 min and holding at 4 °C. A PCR kit (Vazyme, P505-d1) was used following the manufacturer's instructions. A final 50-μL PCR assay contained 0.4 μM forward and reverse primers, 1 ng E. *coli* genomic DNA, and 1X EvaGreen (Biotium) for qPCR. The PCR product was purified with a PCR clean-up kit (Zymo Research) and quantified using a dsDNA quantification Kit (Qubit 1X dsDNA HS).

We used a homebrew mastermix for MDA reactions. A 100-μL aliquot of mastermix contains 35 μL of deionized water, 10 μL of phi29 reaction buffer (Vazyme), 5 μL of phi29 polymerase (Vazyme), 5 μL of random primer (Exo-resistant random primer, Thermo/Finnzymes), 40 μL of dNTP and 5 μL of 20X EvaGreen. To perform the reaction, 0.1 μL E. *coli* genomic DNA (0.5 ng/μL) was added to a 9.9 μL mastermix. 2 μL of the reaction mix was loaded into the microreactor chip for on-chip reaction. The chip was pre-treated with pLL to prevent biomolecule adsorption to channel surfaces. A group of 10-μL tube-based reactions was conducted in parallel to obtain the optical quantification results (Qubit). All the reactions were incubated at 30 °C for 4 h.

2.3. DNA quantification

Unless for the *in situ* MDA monitoring, a homebrew PCR buffer was used in the electrical measurements of *I–V* characteristics. The buffer consists of 10 mM Tris–HCl (pH 8.5), 20 mM KCl, 1.5 mM $MgCl_2$ and 1.5 mM $(NH4)_2SO_4$. Ag/AgCl working and reference electrodes were inserted in corresponding ports of the channels. Purified *E. coli* genomic DNA fragments were diluted in the PCR buffer to the stated concentrations for DNA detection. The DNA solutions were loaded to the sample channel of the device. After incubation (typically 5 min), a sequence of voltage pulses (from −2 V to +2 V at the speed of 40 V/s) was applied using an electrochemical analyzer (CH-Instruments 832D), and the *I–V* characteristics were recorded. To ensure that the adsorption of DNA reaches saturation, an elongated time duration of the DNA incubation (10 min) was used in some experiments. The same process was applied when detecting the primer, dNTP, and polymerase. To refresh the biosensor, a 1 mg/mL pLL (Sigma-Aldrich) solution in PCR buffer was injected into the sample channel and incubated for 5 min at room temperature. The *I–V* characteristics were measured every 30 s during the incubation for the real-time experiment. For the PCR quantification experiments, a 5-μL aliquot of PCR mixtures terminated at the stated cycles was collected and directly loaded to the sample channel of the device without further purification and incubated for 5 min before testing. The same device was used to monitor a complete PCR run with a pLL refreshment step applied between each PCR quantification. Unless for real-time experiments, the sample channel of the device was thoroughly washed (flushing with PCR buffer and incubation for 5 min) to remove any non-absorbed species before *I–V* measurements.

The *I–V* signals were collected every 30 min during a 4-h reaction for MDA monitoring experiments. The device was placed under an inverted fluorescent microscope (Nikon Eclipse Ti2) to capture the fluorescent images at stated time spots. The fluorescence intensities were quantified using the built-in software (NIS-Elements).

3. Results and discussion

3.1. Device characterization

Fig. 2a depicts the overall integrated device and its measurement setup. The device features a hydrogel heterojunction bridging two microchannels. The inset superimposed fluorescent micrograph displays the actual layout of the fabricated hydrogel junction labeled with charged fluorescent dye molecules for illustration purposes. A negatively charged dye, fluorescein, was enriched in the *N*-type gel segment. By contrast, positively charged rhodamine B molecules accumulated in the *P*-type segment. This phenomenon agrees with the electrostatic effects posed by the intrinsic charge of the polymer chains and verifies that the hydrogel heterojunction was successfully patterned. The *P*-type and *N*-type segments were around 100 μm in length and 30 μm in width. We then characterized the integrated ionic diode under a buffer condition relevant to DNA amplification. This is because the rectification behavior of ionic diodes is sensitive to pH and ionic strength [30]. As shown in Fig. 2b, a freshly prepared ionic diode exhibited a reasonable rectification (original state), and the ionic currents at positive voltages were suppressed. To quantify the degree of rectification, we define the ratio between current levels at fixed bias voltages of −2 V (I_{-2V}) and +2 V (I_{+2V}) as rectification ratio (R); $R = |I_{-2V}/I_{+2V}|$. Based on the recorded *I–V* curves, the intact ionic diode owns an R of 4.22 ± 0.53 (n = 8).

We hypothesized that the hydrogel ionic diode should function as a field-effect biosensor whose rectification degree is sensitive to the surface charge density and thus influenced by the adsorption of highly charged biomolecules. To investigate our hypothesis, we introduced a DNA (80 ng/μL of 500 bp *E. coli* genomic DNA) solution to the sample channel. We observed a modulated *I–V* curve whose *R*-value was reduced to 2.6. In a successive experiment, exposing the same device to a cationic polyelectrolyte solution (1 mg/μL pLL) almost recovered the diode to the original state, and an *R*-value of 3.7 was obtained. The results verified that the rectification behavior indeed responded to the charge of adsorbed DNA. The introduced charge could be compensated by an extra layer of oppositely charged polymers. The latter drew our particular attention as it might suggest a simple approach to rejuvenating the biosensor after each measurement. This is essential because the same device can be repeatedly applied to unknown concentrations without considering intrinsic variations across different devices. Similar strategies leveraging layer-by-layer assembles of polyelectrolytes and electrostatic charge overcompensation to recover the sensing surface were reported in previous field-effect biosensors [16,31]. However, charge overcompensation was not observed in our case; that is, the adsorption of DNA did not alter the overall charge polarity of the *N*-type gel. Otherwise, the rectification would be diminished. This is possibly owing to the substantial surface-area-to-volume ratio of the three-dimensional porous hydrogel structure in our case compared to planar surfaces in previous reports and the limited transport of polyelectrolyte chains in the hydrogel matrix. To further investigate the potential sensor rejuvenation capacity, we conducted four consecutive rounds of alternating DNA and pLL depositions on a representative device. Fig. 2c shows the rectification ratio of the device after each step. The preserved and non-degraded cyclic pattern of *R* confirms that the same hydrogel ionic diode can be used for multiple rounds of nucleic acid detection with the simple electrostatic modification being applied. It was found in a previous report that repeated application of polyelectrolyte layer-by-layer assembly could lead to degraded ionic current rectification in 20-nm conical nanopores [32]. The effect was explained by the physical confinement-induced structural reorganization of polyelectrolytes. However, considering the significantly larger pores of the hydrogels determined by scanning electron microscopy (Fig. S2), the effect should be negligible in our ionic diodes.

3.2. Dose-dependent detection of DNA

Having examined the functionality of the hydrogel ionic diodes, we moved to evaluate whether the device could detect DNA in a dose-dependent format. In a preliminary experiment, we monitored the shift in *R* (Δ*R*) relative to its original value of a device being exposed to increasing levels of DNA (500 bp fragments of *E. coli* genomic DNA), Fig. 3a. The DNA solution was injected into the sample channel and incubated for 5 min, after which a new solution was immediately introduced to the device without any washing steps. It can be noted that the rectification level reached a relative plateau at around 3 min after the introduction of DNA. Overall, the shift in rectification aligns with the dose of DNA. We next moved to investigate whether the biosensor responds to the total mass of DNA molecules (mass concentration) or their absolute quantity (mole concentration). A broadly applicable DNA

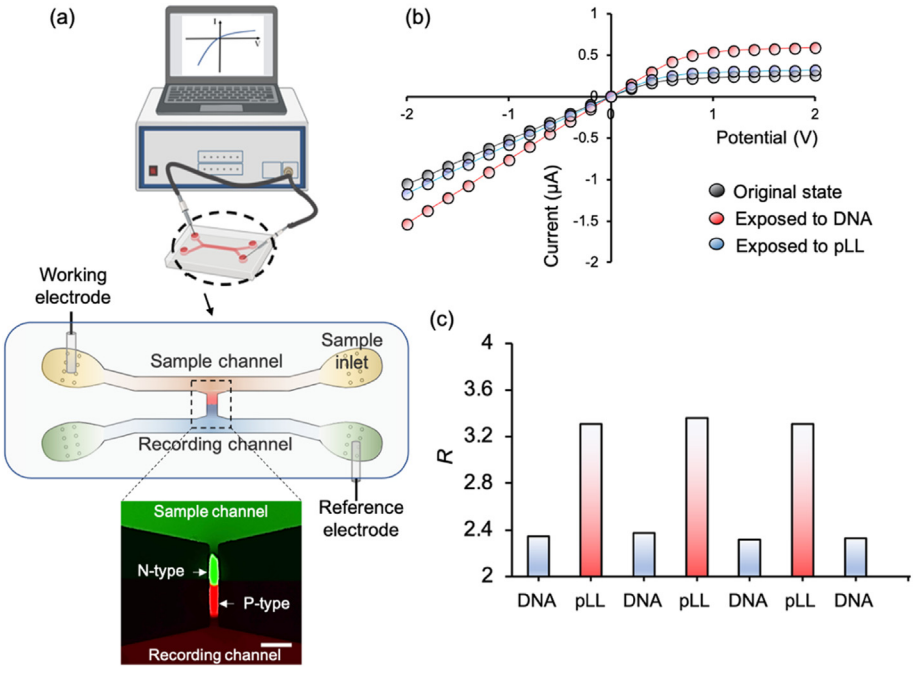

Fig. 2. (a) Schematic presentation of the monolithically integrated ionic diode microchip and the relevant measurement setup. The superimposed fluorescent micrograph displays the hydrogel heterojunction patterned between the sample and recording channels. The polyelectrolyte hydrogel segments are labeled with respective charged dyes for illustration (green: fluorescein, red: rhodamine B). Scale bar: 100 μm. (b) *I–V* curves depicting the initial state of a representative ionic diode device and the states upon sequential exposure to 80 ng/μL negatively charged DNA (500 bp, 10-min incubation) and 1 mg/μL positively charged pLL solutions (5-min incubation). (c) Rectification ratios of a representative device subject to four repeated rounds of DNA and pLL treatments.

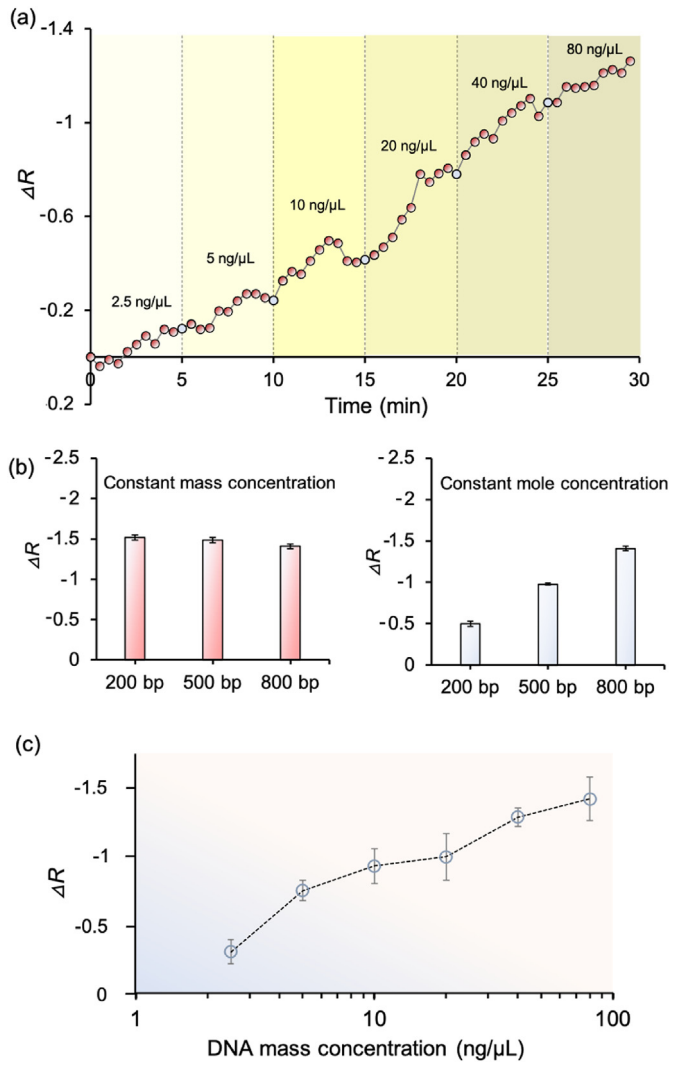

Fig. 3. Dose-sensitive detection of DNA with the ionic diode. (a) A real-time trajectory showing the shift in rectification ratio of a representative ionic diode upon exposure to various mass concentrations of 500-bp DNA fragments. (b) Biosensor response to DNA fragments of varying lengths at constant mass (left) and mole (right) concentrations, respectively. (c) Dose-response plot of the presented ionic diodes based on the shift in rectification ratio as a function of DNA mass concentration (incubation time: 10 min). The symbols and bars in (b) and (c) represent the mean and standard deviation derived from parallel tests using separate devices (n = 3 for b and n = 5 for c).

quantification approach should be sensitive solely to DNA mass concentration to be capable of indistinctively detecting DNAs of vastly different lengths. We fed the diode with 200–800 bp DNA solutions with the same mass concentration of 80 ng/μL and found a negligible difference in the output (Fig. 3b, left). These DNA molecules of equal mole concentration (0.15 μM) yielded markedly varied readouts (Fig. 3b, right). This is expected because the rectification behavior of the ionic diode should be a function of the charge density of the hydrogels; the charge density is a direct reflection of the total base pair number of nucleic acids adsorbed to the gel, *i.e.,* the mass concentration. Based on a series of *I–V* measurements (Fig. S3), we derived the dose-response relation of the developed biosensor, Fig. 3c. A dynamic range of 2.5–80 ng/μL was obtained, similar to the yield of typical nucleic acid amplification assays such as PCR and MDA.

3.3. Monitoring of PCR cycles

Encouraged by the demonstrated dose-responsive behavior, we attempted to utilize the biosensor to monitor the progress of a PCR run in which a 500-bp segment of *E. coli* genomic DNA was amplified. However, besides the double-stranded products, also presented in the PCR mixtures are the single-stranded primers, dNTP, and polymerase. It is essential to rule out any potential influences on the readout posed by these non-target molecules. With this goal, we individually tested them at concentrations identical to PCR using the ionic diodes, Fig. 4a. The primer pairs (0.4 μM each) caused a shift of −0.17 in the rectification ratio. They were, however, ~5 ng/μL in mass concentration, which was expected to induce a Δ*R* of ~ −0.5 according to the calibration curve in Fig. 3c. The discrepancy possibly arises from that a large portion of the primers was

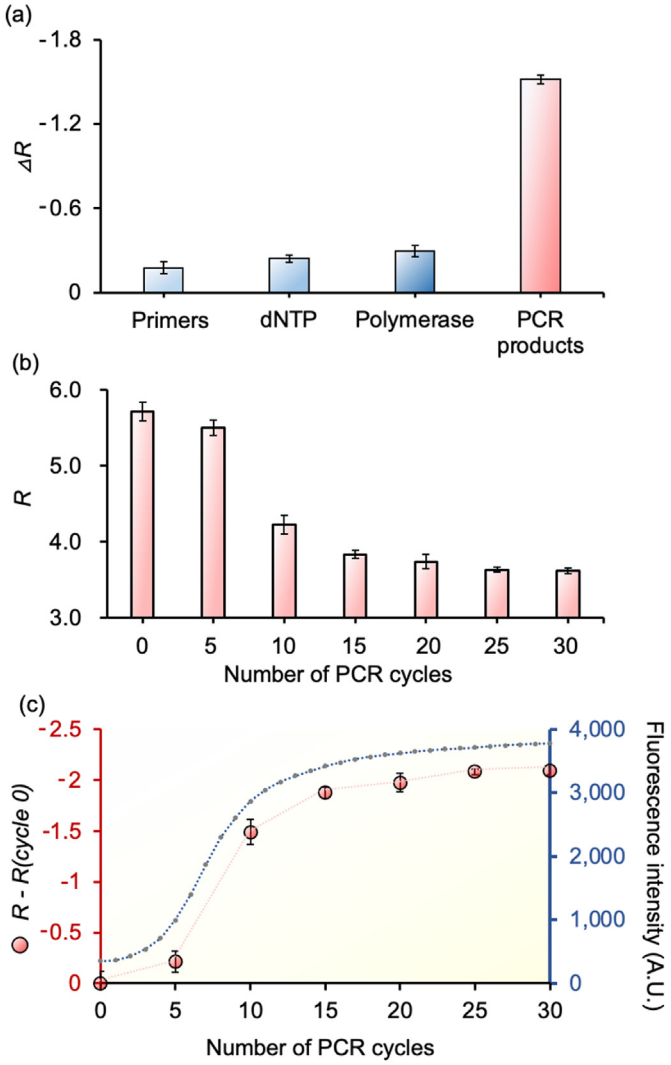

Fig. 4. Monitoring PCR progress with the ionic diode. (a) Changes in rectification ratio induced by individual components in a typical PCR: primers (0.4 μM each), dNTP (50 μM each), polymerase (0.05 units/μL), and purified 500-bp PCR products (80 ng/μL). (b) The rectification ratio of the same device subjected to unpurified PCR products terminated at various cycles. After each test, the ionic rectification behavior of the diode was recovered by treating with pLL. (c) PCR amplification curves obtained electrically from the presented ionic diode (red) and optically from real-time quantitative PCR (blue). The symbols and bars represent the mean and standard deviation derived from three separate *I–V* measurements.

eluted off the hydrogel during washing, indicating that stronger multivalent interactions might be required to realize permanent electrostatic adsorption of DNA on a cationic polymer surface. Likewise, the impacts of dNTPs (50 μM each) and polymerase (0.05 units/μL) were faint. By contrast, a sample of purified 500-bp PCR products, having a mass concentration of ~80 ng/μL, led to a ΔR of ~ −1.5, in excellent alignment with our previous findings (Fig. 3c). These results indicate that the signals arising from the DNA products should be dominant during the amplification reaction. Typical PCR assays include more than 30 thermal cycles. To investigate the effect of elevated temperature on the rectification ratio, we conducted an experiment where an ionic diode device underwent a PCR extension process (72 °C, 3 min) after detecting 80 ng/μL DNA. The rectification behavior of the device only exhibited a minor change (~0.2) after heating (Fig. S4), suggesting that the electrostatic interaction between DNA and hydrogel is adequately strong to immobilize DNA during the thermal cycling. Next, we tested the biosensor response to unpurified PCR mixtures terminated at various cycles, Fig. 4b. As seen, the rectification ratio, derived from *I–V* measurements (Fig. S5a), decreased gradually along with the ongoing PCR and reached saturation after 20 cycles. Note that the *R*-value at 0 cycles (~5.7) was slightly higher than previous values obtained in a homebrew buffer, possibly owing to the difference in ionic strength between the homebrew buffer and the PCR mastermix. To better visualize the trend in rectification behavior, we plotted the rectification shift relative to the *R*-value at cycle 0 as a function of PCR cycles in Fig. 4c. Moreover, the optical quantification curve of an identical PCR obtained using intercalating dye-based real-time quantification was overlaid for comparison. Exhilaratingly, close concordance was found between the electrical and optical outputs. Both the curves exhibited a linear phase between cycles 5 to 10 and a plateau phase from cycle 15. These results suggest that our electrical quantification approach holds a comparable dynamic range and sensitivity to real-time PCR.

3.4. *In situ* real-time monitoring of MDA

Point-of-care diagnosis calls for miniaturized and fully integrated solutions to monitor nucleic acid amplification. Therefore, we modified our original chip design and further integrated a 2-μL reaction chamber directly exposed to the *N*-type gel of the ionic diode built on the side, Fig. 5a. This allowed us to monitor the progress of an isothermal nucleic acid amplification reaction in real-time. To test the utility of the modified device, we performed small-volume MDA reactions amplifying the *E. coli* whole genome. The success of MDA in the miniaturized reaction chamber was first determined optically. We inspected the fluorescence from intercalating dye-labeled dsDNA at both the hydrogel junction and a local area of the reaction chamber. As shown in the micrographs (Fig. 5b, top), the fluorescence within the *N*-gel segment was elevated along time, as well as the fluorescence in the reaction chamber. By contrast, the *P*-type gel remained dim throughout the 4-h reaction. These findings were supported by the fluorescence intensity plot (Fig. 5b, bottom). Notably, the intensity of the *N*-type gel was the highest by the end of the reaction, suggesting a high local concentration of MDA products accumulated within the *N*-gel due to electrostatic associations. Furthermore, the uniform fluorescence across the *N*-gel indicates that the electrostatic adsorption of DNA occurred evenly throughout the hydrogel matrix rather than around the entrance region.

We next monitored the rectification behavior throughout a 4-h MDA reaction at a time interval of half an hour. For comparison, a tube-based reaction was conducted in parallel, and the yield was quantified by a commercial optical means, Qubit. Both the electrical and optical readouts

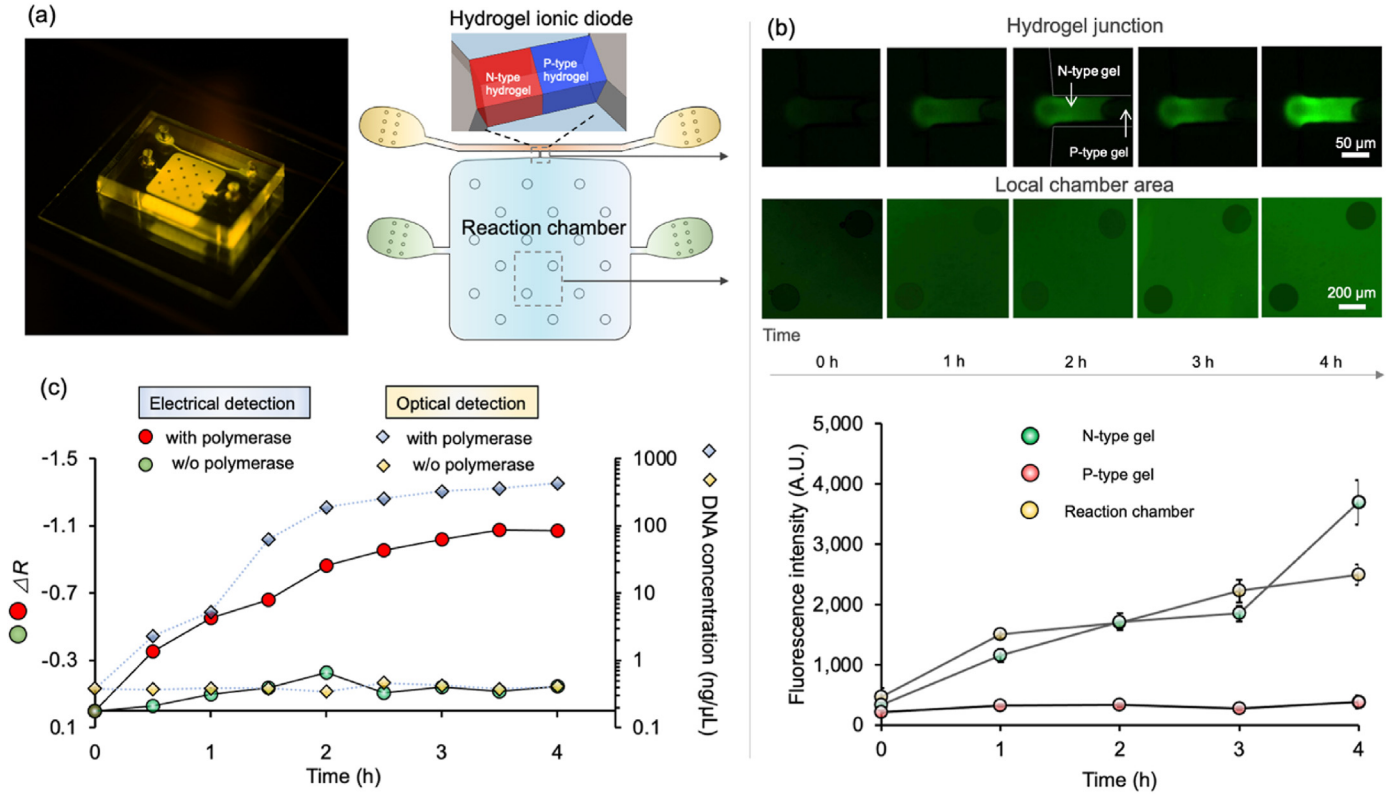

Fig. 5. *In situ* real-time monitoring of an isothermal MDA reaction amplifying *E. coli* whole genome. (a) A modified microchip integrating a 2-μL reaction chamber to accommodate the MDA reaction and an adjacent hydrogel ionic diode for *in situ* monitoring. (b) Fluorescent micrographs (top) and intensity (bottom) of the *N*-type gel, *P*-type gel, and reaction chamber, respectively, during the DNA amplification process. The symbols and bars represent the mean and standard deviation derived from fluorescence measured at different positions (n = 3). (c) The electrical and optical readouts recording the progress of a typical MDA reaction. The electrical readout refers to the shift in the rectification ratio of the ionic diode. The optical readout is measured from a parallel tube-based reaction using a commercial optical instrument, Qubit.

were plotted in Fig. 5c. Note that the DNA concentration of the tube-based MDA might not directly correspond to that in the chip-based reaction chamber, as the efficiency of the two reactions might be slightly different. However, as shown in the plot, they should share similar reaction dynamics because the electrical readout derived from *I–V* measurements (Fig. S5b) aligns closely with the Qubit data. A negative control that excluded the polymerase caused almost no visual signals, suggesting that our ionic sensor detected the accumulated dsDNA products rather than other species existing in the reaction mixture. A further set of MDA monitoring experiments was conducted using three different devices (n = 3) to evaluate the batch errors, and the electrical readouts from the three devices exhibited reasonably good agreement (Fig. S6).

Typical MDA reactions yield dsDNA products of lengths around 10 kb [33]. The demonstrated capability of the ionic diode to detect such long products and the proven success of detecting shorter PCR amplicons (<1 kb) suggests the universal applicability of the presented device towards various nucleic acid amplification techniques. Relying on the electrostatic charge-based field-effect for biosensing, the hydrogel ionic diodes do not require extra labeling steps and probes in DNA amplification detection. The devices, once fabricated, can readily detect DNA with no surface functionalization needed. However, it is worth noting that the given device and related electrical DNA detection strategy lack additional specificity as offered by hybridization-based methods [34]; thus, the specificity in the nucleic acid amplification steps must be strictly controlled to ensure that only the target sequence is amplified. Otherwise, the device will indiscriminately detect the abundance of non-target products and produce false-positive signals. To further eliminate the signals caused by non-target products requires extra functionalization and passivation steps to render the biosensor specific to the target.

The presented ionic diodes utilize polyelectrolyte hydrogel, an intrinsically charged and nano-porous material to construct the field-effect sensor, rather than semiconductor nanowires or nanofluidic channels which require cumbersome fabrication. As a result, the device features convenient fabrication and high cost-effectiveness. It is worth noting that the aperture size of the hydrogels poses a strong impact on the rectification behavior. The relation between the rectification and the pore size of polyelectrolyte hydrogel ionic diodes was studied in a recent report by our group [30]. In brief, the rectification degrades with the increasing size of pores. This is because the ion distribution within the gel is increasingly dominated by the bulk ionic strength, rather than the charge of the hydrogel chains. Therefore, one would expect a decreased sensitivity of the device for detecting DNA if the hydrogel pores are enlarged. The porous nanostructure may also exert a physical barrier effect on the DNA molecules. However, such an effect could only be prominent when the hydraulic size of the DNA is close to the size of the nanopores. In our case where the targets are short DNA amplicons (typically less than 10 kb), the effect should be negligible.

The geometry of the heterojunction is essential to the sensing performance such as sensitivity and limit of detection. Further scaling down the geometry of the junction should lead to enhanced sensitivity to DNA because the reduced sensing volume (the *N*-type gel) requires less amount of DNA molecules to induce distinguishable changes in the rectification level. However, the reduced geometry may also lead to a narrowed dynamic window. This may lead to signal saturation at the early stages of the amplification process.

4. Conclusions

Label-free electrical monitoring of nucleic acid amplification has been demonstrated based on an integrated platform of hydrogel ionic diodes. Although the current format relies on an external instrument for signal recording, further integration of electrical measurement components is trivial given the maturity of compact circuity techniques. A complete version of the device to meet the demand of point-of-care testing should also consider the integration of a sample preparation module towards a micro total analysis system (μTAS). Given the demonstrated performance in monitoring PCR and MDA with simple electrical measurements, convenient sensor recovery, and high cost-effectiveness and manufacturability, the presented monolithic integration of hydrogel ionic diode-based biosensors should be widely applicable in a point-of-care setting.

Author contributions

Chenwei Xiong: Investigation, Methodology, Formal analysis, Writing- Original draft preparation. **Jie Li**, **Luyao Li**, and **Long Chen**: Investigation. **Rong Zhang**: Data Curation, Project administration. **Xianqiang Mi**: Funding acquisition, Supervision. **Yifan Liu**: Conceptualization, Methodology, Supervision, Funding acquisition, Writing - Original draft preparation, Writing - Review & Editing.

Declaration of competing interest

The authors declare that they have no known competing financial interests or personal relationships that could have appeared to influence the work reported in this paper.

Acknowledgements

This work was sponsored by the National Natural Science Foundation of China (Grant No. 61904105) and the Shanghai Academic/Technology Research Leader (Grant No. 20XD1404600). Y. Liu also acknowledges start-up funding support from ShanghaiTech University. The authors appreciate the Soft NanoLab (SNL) and Electron Microscopy Center (EMC) at the School of Physical Science and Technology (SPST), ShanghaiTech University, for technical support.

Appendix A. Supplementary data

Supplementary data to this article can be found online at https://doi.org/10.1016/j.mtbio.2022.100281.

References

[1] M. Ackermann, S.E. Verleden, M. Kuehnel, A. Haverich, T. Welte, F. Laenger, A. Vanstapel, C. Werlein, H. Stark, A. Tzankov, W.W. Li, V.W. Li, S.J. Mentzer, D. Jonigk, Pulmonary vascular endothelialitis, thrombosis, and angiogenesis in covid-19, N. Engl. J. Med. 383 (2) (2020) 120–128, https://doi.org/10.1056/NEJMoa2015432.

[2] M. Shen, Y. Zhou, J. Ye, A.A. Abdullah Al-Maskri, Y. Kang, S. Zeng, S. Cai, Recent advances and perspectives of nucleic acid detection for coronavirus, J Pharm Anal 10 (2) (2020) 97–101, https://doi.org/10.1016/j.jpha.2020.02.010.

[3] J.J. Mridu Sinhaa, Hannah Macka, P. Todd, f Colemana, M. Shelley, d e f Lawrencec, Stephanie I. Fraleya e f, Emerging technologies for molecular diagnosis of sepsis, Clin. Microbiol. Rev. 31 (2018), e00089.

[4] A. Tahamtan, A. Ardebili, Real-time RT-PCR in COVID-19 detection: issues affecting the results, Expert Rev. Mol. Diagn 20 (5) (2020) 453–454, https://doi.org/10.1080/14737159.2020.1757437.

[5] M.J. Kellner, J.G. Koob, J.S. Gootenberg, O.O. Abudayyeh, F. Zhang, SHERLOCK: nucleic acid detection with CRISPR nucleases, Nat. Protoc. 14 (10) (2019) 2986–3012, https://doi.org/10.1038/s41596-019-0210-2.

[6] S.B. He, J.X. Tian, X.D. Li, Y.N. Zhou, M.Z. Xiao, Y. Zhang, X.J. Min, X.Y. Li, D. Jin, Q. Zhang, Y.J. Zheng, J. Ke, Q.W. Li, J.X. Tao, P. Song, H. Wang, Y. Lv, Q.Y. Ding, S. Tang, J.R. Lin, Z.Y. Jiang, Z.J. Zhang, J.X. Song, F.M. Lian, X.L. Tong, Positive RT-PCR test results in 420 patients recovered from COVID-19 in wuhan: an observational study, Front. Pharmacol. 11 (2020) https://doi.org/ARTN 54911710.3389/fphar.2020.549117.

[7] D. Liu, H.C. Shen, Y.Q. Zhang, D.Y. Shen, M.Y. Zhu, Y.L. Song, Z. Zhu, C.Y. Yang, A microfluidic-integrated lateral flow recombinase polymerase amplification (MI-IF-RPA) assay for rapid COVID-19 detection, Lab Chip 21 (10) (2021) 2019–2026, https://doi.org/10.1039/d0lc01222j.

[8] S.J. Li, W.J. Jiang, J.F. Huang, Y. Liu, L.J. Ren, L. Zhuang, Q.N. Zheng, M. Wang, R. Yang, Y. Zeng, Y. Wang, Highly sensitive and specific diagnosis of COVID-19 by reverse transcription multiple cross-displacement amplification-labelled nanoparticles biosensor, Eur. Respir. J. 56 (6) (2020) https://doi.org/Artn 200206010.1183/13993003.02060-2020.

[9] N. Peker, N. Couto, B. Sinha, J.W. Rossen, Diagnosis of bloodstream infections from positive blood cultures and directly from blood samples: recent developments in molecular approaches, Clin. Microbiol. Infect. 24 (9) (2018) 944–955, https://doi.org/10.1016/j.cmi.2018.05.007.

[10] B.B. Oliveira, B. Veigas, P.V. Baptista, Isothermal amplification of nucleic acids: the race for the next "gold standard", Frontiers in Sensors 2 (2021) https://doi.org/10.3389/fsens.2021.752600.
[11] H. Gudnason, M. Dufva, D.D. Bang, A. Wolff, Comparison of multiple DNA dyes for real-time PCR: effects of dye concentration and sequence composition on DNA amplification and melting temperature, Nucleic Acids Res. 35 (19) (2007) https://doi.org/ARTN e127 10.1093/nar/gkm671.
[12] N.S. Green, M.L. Norton, Interactions of DNA with graphene and sensing applications of graphene field-effect transistor devices: a review, Anal. Chim. Acta 853 (2015) 127–142, https://doi.org/10.1016/j.aca.2014.10.023.
[13] G. Xu, J. Abbott, D. Ham, Optimization of CMOS-ISFET-based biomolecular sensing: analysis and demonstration in DNA detection, IEEE Trans. Electron. Dev. (2016) 1–8, https://doi.org/10.1109/ted.2016.2582845.
[14] C. Duarte-Guevara, Vikhram V. Swaminathan, B. Reddy, J.-C. Huang, Y.-S. Liu, R. Bashir, On-chip electrical detection of parallel loop-mediated isothermal amplification with DG-BioFETs for the detection of foodborne bacterial pathogens, RSC Adv. 6 (106) (2016) 103872–103887, https://doi.org/10.1039/c6ra19685c.
[15] V.F. Anurup Ganguli, Ariana Mostafa, Michael T. Hwang, Seungyong You, Rashid Bashir, High sensitivity graphene field effect transistor-based detection of DNA amplification, Adv. Funct. Mater. 30 (2020) 2001031.
[16] Y. Liu, L. Yobas, Label-free electrical quantification of amplified nucleic acids through nanofluidic diodes, Biosens. Bioelectron. 50 (2013) 78–83, https://doi.org/10.1016/j.bios.2013.06.013.
[17] M.Y. Shen, B.R. Li, Y.K. Li, Silicon nanowire field-effect-transistor based biosensors: from sensitive to ultra-sensitive, Biosens. Bioelectron. 60 (2014) 101–111, https://doi.org/10.1016/j.bios.2014.03.057.
[18] R. Stine, J.T. Robinson, P.E. Sheehan, C.R. Tamanaha, Real-time DNA detection using reduced graphene oxide field effect transistors, Adv. Mater. 22 (46) (2010) 5297–5300, https://doi.org/10.1002/adma.201002121.
[19] Z. Wang, Y. Liu, L. Yu, Y. Li, G. Qian, S. Chang, Nanopipettes: a potential tool for DNA detection, Analyst 144 (17) (2019) 5037–5047, https://doi.org/10.1039/c9an00633h.
[20] A. Ganguli, V. Faramarzi, A. Mostafa, M.T. Hwang, S. You, R. Bashir, High sensitivity graphene field effect transistor-based detection of DNA amplification, Adv. Funct. Mater. 30 (28) (2020) https://doi.org/ARTN 200103110.1002/adfm.202001031.
[21] Y.F. Liu, L. Yobas, Slowing DNA translocation in a nanofluidic field-effect transistor, ACS Nano 10 (4) (2016) 3985–3994, https://doi.org/10.1021/acsnano.6b00610.
[22] B.R. Putra, L. Tshwenya, M.A. Buckingham, J.Y. Chen, K.J. Aoki, K. Mathwig, O.A. Arotiba, A.K. Thompson, Z.K. Li, F. Marken, Microscale ionic diodes: an overview, Electroanal 33 (6) (2021) 1398–1418, https://doi.org/10.1002/elan.202060614.
[23] Y.F. Wu, D.Y. Wang, I. Willner, Y. Tian, L. Jiang, Smart DNA hydrogel integrated nanochannels with high ion flux and adjustable selective ionic transport, Angew. Chem. Int. Ed. 57 (26) (2018) 7790–7794, https://doi.org/10.1002/anie.201803222.
[24] T.T. Tran, A. Mulchandani, Carbon nanotubes and graphene nano field-effect transistor-based biosensors, Trac. Trends Anal. Chem. 79 (2016) 222–232, https://doi.org/10.1016/j.trac.2015.12.002.
[25] D. Sarkar, W. Liu, X.J. Xie, A.C. Anselmo, S. Mitragotri, K. Banerjee, MoS2 field-effect transistor for next-generation label-free biosensors, ACS Nano 8 (4) (2014) 3992–4003, https://doi.org/10.1021/nn5009148.
[26] H.G. Chun, T.D. Chung, Iontronics, Annu Rev Anal Chem 8 (2015) 441–462, https://doi.org/10.1146/annurev-anchem-071114-040202.
[27] J.H. Han, K.B. Kim, H.C. Kim, T.D. Chung, Ionic circuits based on polyelectrolyte diodes on a microchip, Angew. Chem. Int. Ed. 48 (21) (2009) 3830–3833, https://doi.org/10.1002/anie.200900045.
[28] H.-R. Lee, J. Woo, S.H. Han, S.-M. Lim, S. Lim, Y.-W. Kang, W.J. Song, J.-M. Park, T.D. Chung, Y.-C. Joo, J.-Y. Sun, A stretchable ionic diode from copolyelectrolyte hydrogels with methacrylated polysaccharides, Adv. Funct. Mater. 29 (4) (2019), https://doi.org/10.1002/adfm.201806909.
[29] S.M. Lim, H. Yoo, M.A. Oh, S.H. Han, H.R. Lee, T.D. Chung, Y.C. Joo, J.Y. Sun, Ion-to-ion amplification through an open-junction ionic diode, P Natl Acad Sci USA 116 (28) (2019) 13807–13815, https://doi.org/10.1073/pnas.1903900116.
[30] C. Xiong, B. Zhang, R. Zhang, Y. Liu, An experimental and numerical study of polyelectrolyte hydrogel ionic diodes: towards electrical detection of charged biomolecules, Sensors 21 (24) (2021), https://doi.org/10.3390/s21248279.
[31] C.S.J. Hou, N. Milovic, M. Godin, P.R. Russo, R. Chakrabarti, S.R. Manalis, Label-free microelectronic PCR quantification, Anal. Chem. 78 (8) (2006) 2526–2531, https://doi.org/10.1021/ac0520689.
[32] M. Ali, B. Yameen, J. Cervera, P. Ramirez, R. Neumann, W. Ensinger, W. Knoll, O. Azzaroni, Layer-by-Layer assembly of polyelectrolytes into ionic current rectifying solid-state nanopores: insights from theory and experiment, J. Am. Chem. Soc. 132 (24) (2010) 8338–8348, https://doi.org/10.1021/ja101014y.
[33] F.B. Dean, S. Hosono, L.H. Fang, X.H. Wu, A.F. Faruqi, P. Bray-Ward, Z.Y. Sun, Q.L. Zong, Y.F. Du, J. Du, M. Driscoll, W.M. Song, S.F. Kingsmore, M. Egholm, R.S. Lasken, Comprehensive human genome amplification using multiple displacement amplification, P Natl Acad Sci USA 99 (8) (2002) 5261–5266, https://doi.org/10.1073/pnas.082089499.
[34] B.J. Cai, S.T. Wang, L. Huang, Y. Ning, Z.Y. Zhang, G.J. Zhang, Ultrasensitive label-free detection of PNA-DNA hybridization by reduced graphene oxide field-effect transistor biosensor, ACS Nano 8 (3) (2014) 2632–2638, https://doi.org/10.1021/nn4063424.